



HAL
open science

Development of decision support tools by model order reduction for active endovascular navigation

Arif Badrou, Arnaud Duval, Jérôme Szewczyk, Raphaël Blanc, Nicolas Tardif, Nahiene Hamila, Anthony Gravouil, Aline Bel-Brunon

► To cite this version:

Arif Badrou, Arnaud Duval, Jérôme Szewczyk, Raphaël Blanc, Nicolas Tardif, et al.. Development of decision support tools by model order reduction for active endovascular navigation. 2022. hal-03858565v1

HAL Id: hal-03858565

<https://hal.science/hal-03858565v1>

Preprint submitted on 17 Nov 2022 (v1), last revised 4 Jan 2024 (v3)

HAL is a multi-disciplinary open access archive for the deposit and dissemination of scientific research documents, whether they are published or not. The documents may come from teaching and research institutions in France or abroad, or from public or private research centers.

L'archive ouverte pluridisciplinaire **HAL**, est destinée au dépôt et à la diffusion de documents scientifiques de niveau recherche, publiés ou non, émanant des établissements d'enseignement et de recherche français ou étrangers, des laboratoires publics ou privés.



Distributed under a Creative Commons Attribution 4.0 International License

Development of decision support tools by model order reduction for active endovascular navigation

Original article

Arif BADROU^a, Arnaud DUVAL^a, Jérôme SZEWCZYK^{b,c}, Raphaël BLANC^{b,d}, Nicolas TARDIF^a, Nahiène HAMILA^e, Anthony GRAVOUIL^a,
Aline BEL-BRUNON^a

^a*Univ Lyon, INSA Lyon, CNRS, LaMCoS, UMR5259, 69621 Villeurbanne, France*

^b*BaseCamp Vascular (BCV), 75005 Paris, France*

^c*Sorbonne Université, CNRS, INSERM, Institut des Systèmes Intelligents et de Robotique, ISIR, ISIR - AGATHE, F-75005 Paris, France*

^d*Department of Interventional Neuroradiology, Fondation Rothschild Hospital, Paris, France*

^e*Ecole Nationale d'Ingénieurs de Brest, ENIB, UMR CNRS 6027, IRDL, F-29200, Brest, France*

Abstract

Endovascular therapies have grown significantly in the recent years. The first step is to reach the ares to treat. However, some trajectories are so-called complex (e.g. Supra-Aortic Trunks (SATs)). In order to facilitate the access to complex targets during catheterization, the French company BaseCamp Vascular (BCV) developed an active guidewire made of Shape Memory Alloy. Our study focused on the navigation of this device and associated catheters to treat neurovascular pathologies through the left carotid artery. For a given anatomy, two problems remain to be overcome: (i) to improve the design of the active guidewire by determining the number of actuators needed

*Corresponding author: Aline Bel-Brunon

Email address: `aline.bel-brunon@insa-lyon.fr` (Aline BEL-BRUNON)

and their curvature and (ii) to propose navigation sequences maximizing the chances of accessing the areas to treat. In a previous study, a finite element model was developed to represent the navigation of the active guidewire and catheters from the aortic arch to the hooking of the left carotid artery of patient-specific aortas. Even if the model is able to represent both a particular design and navigation of the aforementioned tools, numerical simulations are time-consuming and cannot be used directly in the clinic routine to provide navigation assistance. Therefore, proofs of concept of numerical charts were developed in this study. Design as well as decision support tools have been developed, allowing to simulate in real-time the performance and the navigation of the active guidewire in a particular anatomy.

Keywords: Model Order Reduction, Numerical chart, Endovascular, Catheters, Guidewire, Aorta

1 **1. Introduction**

2 Endovascular therapies have grown significantly in the recent years. It is
3 estimated that in 2026, 80% of cardiovascular problems will be treated by
4 endovascular therapies [1]. The first step to treat endovascular pathologies is
5 to reach the concerned area. However, clinicians may be confronted with so-
6 called complex pathways (e.g. renal arteries or Supra-Aortic Trunks (SATs)).
7 It is also estimated that 20% endovascular therapies present these complexi-
8 ties which may compromise the continuation of the intervention [2]. In order
9 to facilitate the access to complex targets through catheterization, the French
10 company BaseCamp Vascular (BCV) developed an active guidewire made of
11 Shape Memory Alloy. The distal tip of this device can curve under an electric

12 impulse and allows to reach complex targets.

13 Our study focused on the access to neurovascular pathologies through
14 the left carotid artery using the active guidewire and associated catheters.
15 The access to the brain areas is facilitated using the active guidewire but
16 two obstacles are to be overcome for a given anatomy: (i) to improve the
17 design of the active guidewire by determining the number of actuators needed
18 and their curvature and (ii) to propose navigation sequences maximizing the
19 chances of accessing the areas to treat. A finite element model was developed
20 to represent the navigation of the active guidewire and catheters from the
21 aortic arch to the hooking of the left carotid artery of patient-specific aortas
22 [3]. The numerical model offers the possibility to test particular guidewire
23 configurations and navigation sequences with a certain representativity.

24 However, numerical simulations are time-consuming and cannot be used
25 directly in the clinic routine to provide navigation assistance. An alternative
26 is to develop numerical charts allowing to explore in a continuous way a wide
27 range of parameters while circumventing the problem of the computational
28 cost.

29 Numerical charts are built using Model Order Reduction (MOR) tech-
30 niques. Two families of MOR are commonly used. The methods known as
31 POD (Proper Orthogonal Decomposition) which require calculations in an
32 offline phase (in the learning phase) allowing the reduction and resolution
33 in a reduced base online (in real-time). In biomechanics and in particular
34 for vascular problems, POD is used for example to process hemodynamic
35 data [4, 5, 6] or to reduce the computational time of complex models [7].
36 The other family concerns the methods known as PGD (Proper Generalized

37 Decomposition) based on the separation of variables, which do not require
38 upstream calculations. In particular, PGD is used for inverse problem solv-
39 ing: in [8] PGD was used to speed up the process of identifying conductivities
40 of heart tissue. Other works have used PGD for computational surgery, let's
41 cite [9, 10, 11] for example. One of the limitations of POD is that it is
42 not adapted to non-linear problems (large strains in particular) and that
43 the enrichment of the reduced bases can quickly become expensive for high
44 dimensional problems and/or with relatively large parameter intervals. By
45 considering uniform grids, the number of snapshots are exponential. For
46 example, for a uniform grid of snapshots in a space of 8 parameters with
47 some 10 values to be considered in each direction, it would take 10^8 finite
48 element calculations. We then speak of *curse of dimensionality*. The PGD
49 allows to overcome this problem since no snapshot is required. However,
50 it remains an intrusive method and is therefore not adapted to the use of
51 commercial softwares. The method used in this study is the HOPGD (High
52 Order Proper Generalized Decomposition) [12]. It is an a posteriori defini-
53 tion of the PGD and has been used to produce 10D numerical charts in the
54 context of real-time numerical simulation of welding processes [13].

55 We first present the active guidewire and the numerical model of endovas-
56 cular navigation. Then, the HOPGD is briefly presented and the methods
57 for the development of numerical charts are explained. Proofs of concept of
58 these charts in order to help clinicians during endovascular therapies are pre-
59 sented. To the best of our knowledge, this is the first study dealing with this
60 kind of numerical tools in a biomedical framework. The results are finally
61 discussed in a last part.

62 **2. Methods**

63 *2.1. The numerical model of the navigation of surgical tools*

64 *2.1.1. The active guidewire and the phantom aorta test bench*

65 The active guidewire is composed of a long shaft in steel. As its end, a
66 blade is attached and Nitinol wires are positioned on both sides of the blade.
67 The ends of the wires are connected to electric wires. A handle allows to
68 transmit an electric impulse to the Nitinol wires and by shape memory effect,
69 the wires shrinks causing the blade to bend [14, 15]. When two Nitinol wires
70 are used, the distal tip of the active guidewire draws a S-shape to facilitate
71 the endovascular navigation (see Fig.1).

72 The active device and catheters are tested on a phantom aorta test bench
73 illustrated in Fig.1. The set-up is composed of a patient-specific aortic arch
74 which can be changed and a fixed cylinder representing the descending aorta.

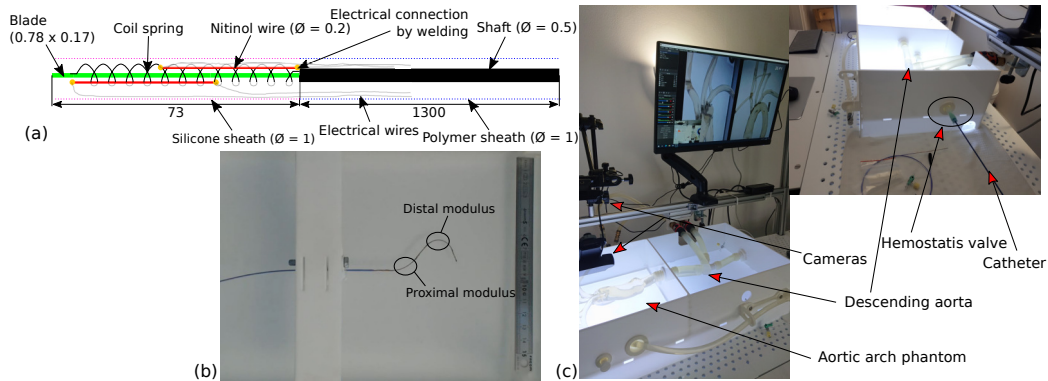


Figure 1: (a) Scheme of the active guidewire developed by BCV with two Nitinol wires placed on both sides of the blade and (b) its activation highlighting the proximal and the distal moduli. (c) Phantom aorta test bench used to test surgical tools in patient-specific aortas.

75 *2.1.2. The numerical model of endovascular navigation*

76 The numerical model simulates the endovascular navigation of the active
77 guidewire and associated catheters in the aorta test bench in Ls-Dyna (LSTC
78 / ANSYS, USA). In the model, the active guidewire is simplified and repre-
79 sented by a long shaft with the blade. The Nitinol wires are placed on both
80 sides of the blade and connected by rigid links. The guidewire is meshed with
81 Hughes-Liu beam elements and the catheters with Belytschko-Tsay shell el-
82 ements. The meshes were defined by convergence analysis and are visible
83 in Fig.2. The mechanical properties of the tools are either hypoelastic or
84 hypoviscoelastic depending on the different areas. The constitutive law for
85 hypoelasticity relates, in Eulerian form, the objective Jaumann derivative of
86 the Cauchy stress tensor σ to the the strain rate tensor \mathbf{D} by the elasticity
87 tensor \mathbf{C} such that :

$$\sigma^\nabla = \mathbf{C} : \mathbf{D} \quad (1)$$

88

89 The tensor \mathbf{C} can be decomposed into a spherical part \mathbf{C}^{sph} and a devi-
90 atoric part \mathbf{C}^{dev} such that:

$$\mathbf{C} = 3K\mathbf{C}^{sph} + 2G\mathbf{C}^{dev} \quad (2)$$

91

92 With K the bulk modulus and G the shear modulus. The hypoviscoelastic
93 properties are modeled with the following law defined in [16]:

$$G(t) = G_\infty + (G_0 - G_\infty)e^{-\beta t}$$

94

95 Where G_∞ and G_0 are respectively the long and short time shear modulus,
96 the parameter β is a constant expressed per unit of time.

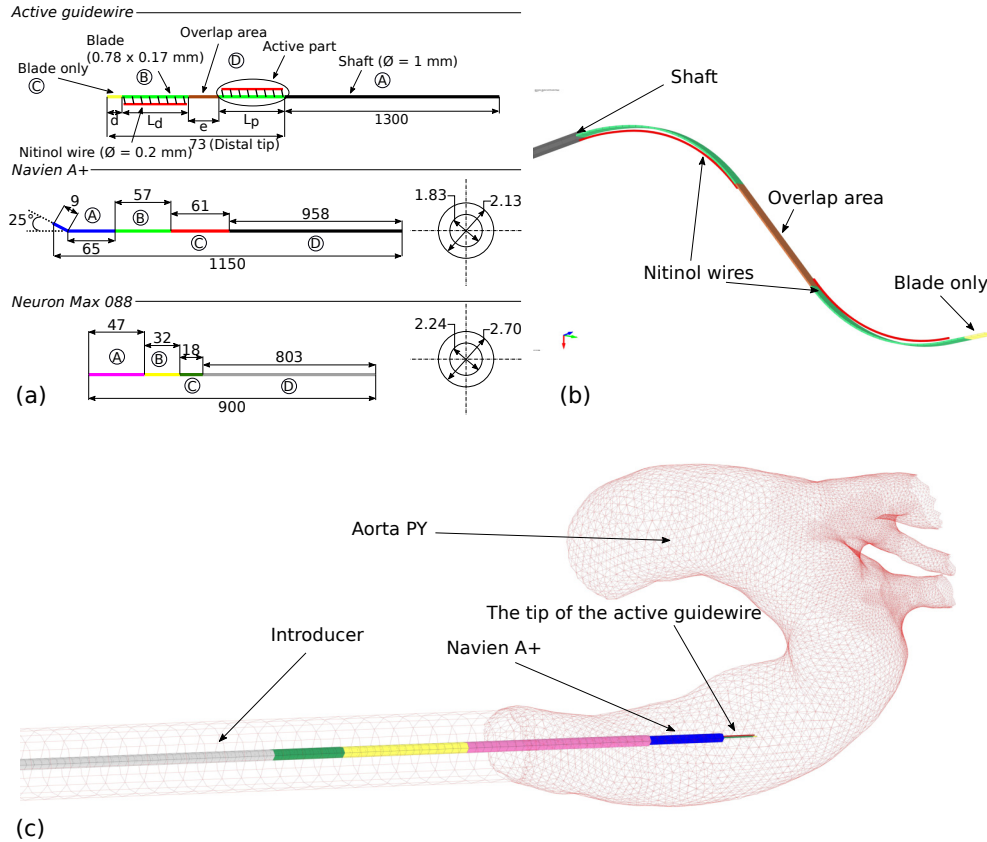


Figure 2: (a) Dimensions of the active guidewire and associated catheters. Each portion of the different tools is defined by a colour and has its own mechanical properties. (b) Activation of the device with two moduli. When the Nitinol wires are heated, they contract resulting in the S-shape bending. (c) Assembly of the different tools in the aorta. The aortic arch is a patient-specific anatomy while the descending aorta is represented by a rigid cylinder.

97

In Fig.1, the mechanical properties and the dimensions of the different

98 tools used in this study are defined. The activation of the guidewire is sim-
99 plified and produced by a displacement command as explained in [3]. The
100 aorta is modeled with shell elements and is rigid considering the navigation
101 into the phantom aorta made of silicone. The patient-specific aorta is also
102 visible in Fig.2. The model was validated as described in [3] by confronting
103 experimental navigation in patient-specific aortas.

Table 1: Mechanical properties along the surgical tools: areas A to D are related to those in Fig.2.

	A	B	C	D
Active guidewire	$E = 8047.8 \text{ MPa}$ $\nu = 0.3$	$E = 71130.0 \text{ MPa}$ $\nu = 0.3$	$E = 52720.0 \text{ MPa}$ $\nu = 0.3$	$E = 175000.0 \text{ MPa}$ $\nu = 0.3$
Navien	$\beta = 0.22 \text{ s}^{-1}$ $G_0 = 62.0 \text{ MPa}$ $G_\infty = 15.9 \text{ MPa}$ $K = 82.9 \text{ MPa}$	$\beta = 0.16 \text{ s}^{-1}$ $G_0 = 94.1 \text{ MPa}$ $G_\infty = 26.6 \text{ MPa}$ $K = 152.3 \text{ MPa}$	$\beta = 0.18 \text{ s}^{-1}$ $G_0 = 448.1 \text{ MPa}$ $G_\infty = 152.2 \text{ MPa}$ $K = 694.6 \text{ MPa}$	$E = 1519 \text{ MPa}$
Neuron	$\beta = 0.26 \text{ s}^{-1}$ $G_0 = 74.0 \text{ MPa}$ $G_\infty = 17.0 \text{ MPa}$ $K = 122.1 \text{ MPa}$	$E = 250 \text{ MPa}$	$E = 180 \text{ MPa}$	$E = 1701 \text{ MPa}$

104 The model is able to reproduce the main movements and phenomena oc-
105 ccurring when it comes to active navigation: translation of the guidewire and
106 the catheter, rotation of the guidewire and particular effect as the snapping
107 explained Fig.3.

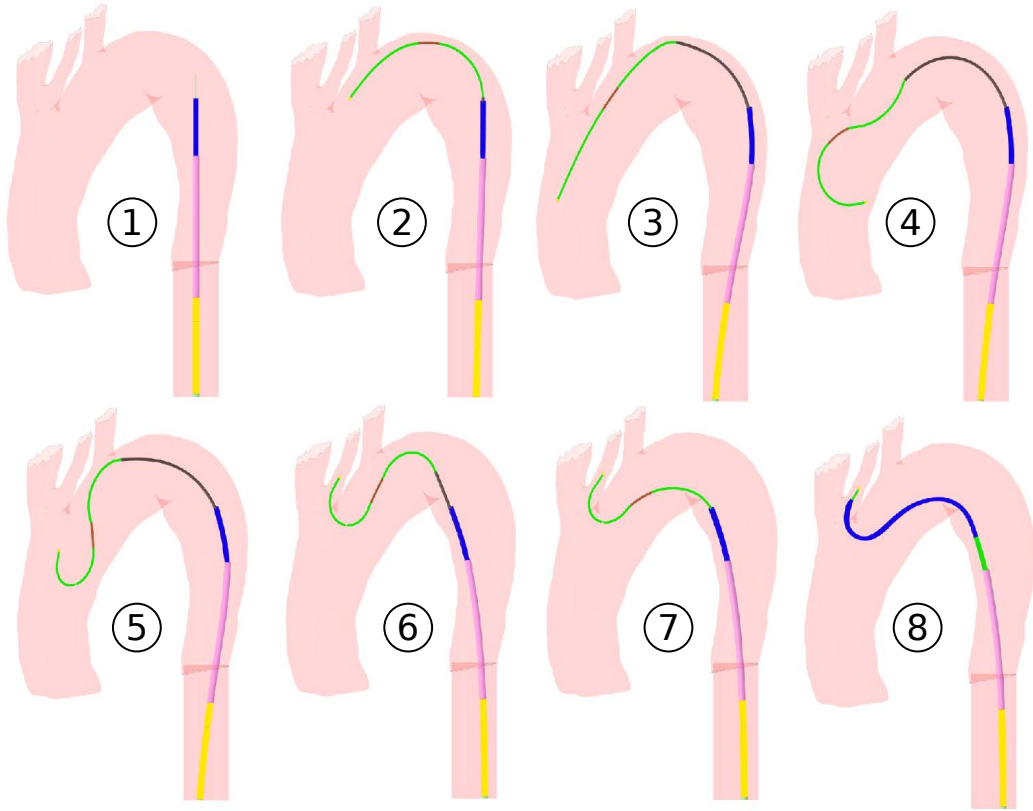


Figure 3: From ① to ③ the guidewire is initially pushed near the left carotid artery entrance. The two modules are activated in ④ while a rotation gesture is applied at the end of the active guidewire. As a consequence, the snapping effect appears(⑤) allowing to point the distal part of the guidewire in the desired direction and to stabilize the device. The guidewire is pulled from ⑥ to ⑦ to straighten the catheters with a deactivation of the proximal module to further tension it. Finally, the catheter slides over the guidewire until it reaches the left carotid artery in ⑧.

108 *2.2. Development of numerical charts*

109 *2.2.1. HOPGD method*

110 We consider a function u dependent on parameters $p_{i=1,d}$ which can be
 111 time, space or control parameters of the problem. These parameters are as-

112 simulated to extra-coordinates of the solution and discretized in the parameter
 113 space. For each set of parameters, HOPGD looks for an approximate form
 114 u^n of u such that:

$$u(p_1, \dots, p_d) \approx u^n(p_1, \dots, p_d) = \sum_{j=1}^n \prod_{i=1}^d F_i^j(p_i) \quad (3)$$

115 n is the order of approximation and the functions $F_{i=1,d}^j$ are related to
 116 the j -th mode. These functions are determined by solving the minimization
 117 problem which consists in looking for $u^n \in V_n \subset \mathcal{L}^2(\Omega)$ minimizing the cost
 118 function J such that:

$$J(u^n) = \min_{u^n \in V_n} \left(\frac{1}{2} \| u^n - u \|^2_{\mathcal{L}^2(\Omega)} \right) \quad (4)$$

119 This minimization problem can be solved by an alternating fixed point
 120 algorithm. For a new set of parameters, the new functions F_i are linearly
 121 interpolated from the existing functions. In this study, the used version of the
 122 HOPGD algorithm does not use snapshot selection by *sparse grids* method
 123 as introduced in [17]. Thus, the discretization of the parameters is conducted
 124 using uniform grids. In Fig.4, the general procedure of the HOPGD method
 125 is illustrated.

126 2.2.2. Parameters

127 The endovascular navigation implies many parameters. They can be
 128 classified into three categories: (i) those related to the design of the active
 129 guidewire (e.g., lengths of the active moduli or distance between them), (ii)
 130 the parameters concerning navigation as activation times or pushing / pulling
 131 times of the surgical tools and (iii) those dealing with geometric parameters

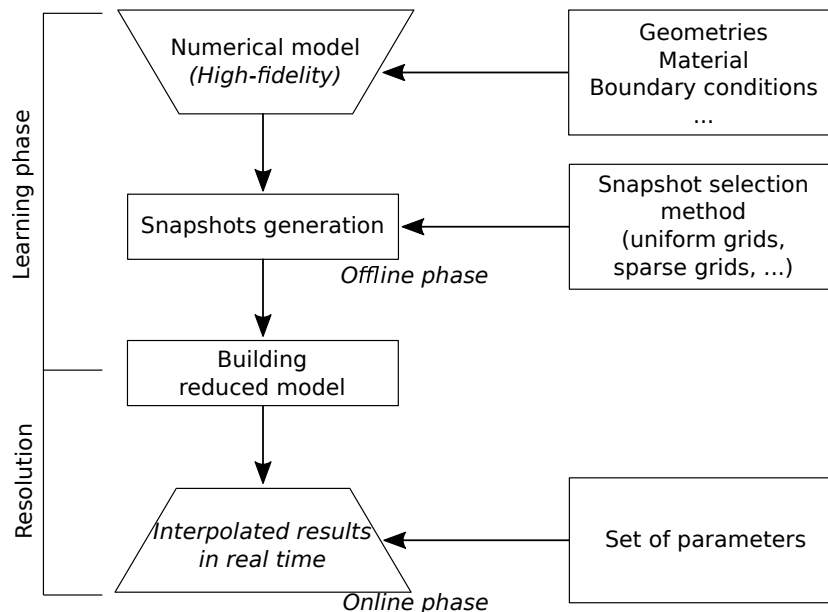


Figure 4: General procedure of the HOPGD method: starting from a high-fidelity numerical model, the different steps lead to the creation of a reduced model capable of providing a real-time response for a given set of parameters.

132 (patient-specific aortas). In our study, we decided to work with fixed geome-
 133 try, i.e. the parameters concern the design of the active guidewire and those
 134 related to the clinician gestures during the navigation. In the following, two
 135 types of numerical charts are presented. First, an active guidewire design
 136 aid tool with five control parameters that are related to the device design
 137 is presented. This tool allows to observe the performance of the activated
 138 guidewire for a given set of parameters. Then, considering the design and
 139 navigation parameters, decision support numerical charts are also proposed
 140 with seven control parameters.

141 *2.2.3. Active guidewire design tool*

142 This first tool aims to provide a design aid tool. From a given guidewire
143 configuration, the tool has to be able to represent in real time the deformation
144 of the guidewire after activation of the moduli.

145 *2.2.3.1. Simulation of the activation of the active guidewire.*

146 The model used to produce the snapshots is presented Fig.5. and consists in
147 simulating the activation of the guidewire. The computational time for such
148 a simulation is about 5 minutes. The output data are the displacements (in
149 X, Y and Z) of the nodes of the distal part of the guide (73 mm blade of
150 the active guide) at the end of the simulation. In other words, the output
151 of each snapshot defines the distal guide deformation for a given guidewire
152 configuration.

153 *2.2.3.2. Choice of parameters.*

154 There are five design parameters in the guidewire for the development of
155 the design support tool in accordance with Fig.5: the lengths L_p , L_d and
156 e that are the lengths of the active moduli and the distance between them,
157 respectively. The parameters ϵ_L for the two Nitinol wires are also considered.
158 The latter are the recoverable strain for the Nitinol wires in the shape memory
159 effect loop representing the wire performances (change in current intensity
160 or Nitinol grade for example). Fig.5 also describes the parameter ranges.

161 *2.2.3.3. Snapshots selection.*

162 As explained, the version of HOPGD we use does not work with the sparse
163 grids method and therefore does not allow for optimal selection of snapshots
164 in the parameter space. Thus, it is chosen for this numerical chart to build

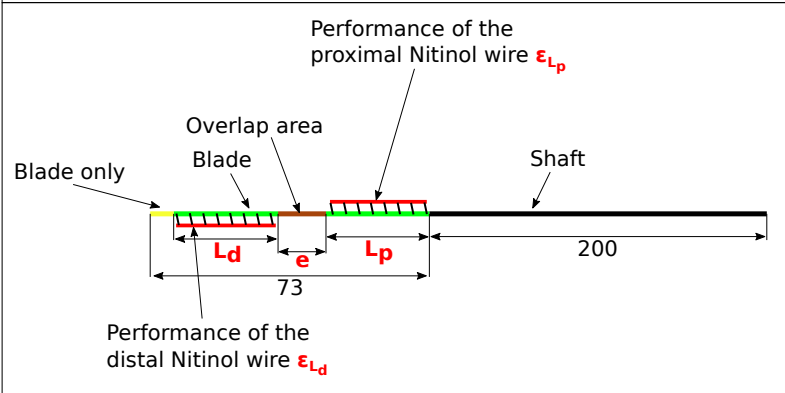
Model of the active guidewire and highlighting of the design parameters	Parameters
	$L_p \in [15;20]$ (mm) $e \in [5;10]$ (mm) $L_d \in [15;40]$ (mm) $\epsilon_{L_p} \in [0.01;0.0347]$ $\epsilon_{L_d} \in [0.01;0.0347]$

Figure 5: Double stage guidewire activation model. The shaft is embedded and a temperature control is applied to both moduli to activate alongside with the ranges of values taken by the design parameters chosen for the design aid chart.

165 a uniform grid with a discretization of three values per parameter (extremal
166 values and middle of each interval on Fig.5, that is to say a grid of $3^5 = 243$
167 finite element calculations that feed the HOPGD method to create the re-
168 duced model. A MatLab (MathWorks, USA) routine is used to automatically
169 create the snapshots with the design parameters of the guide as input data.
170 Once the snapshots are computed, the HOPGD algorithm is used to build
171 the reduced model with a default number of modes fixed at 20.

172 2.2.3.4. Evaluation of the error.

173 For this numerical chart, we evaluate the accuracy of the reduced model.
174 So-called evaluation points are then selected in the center of the subdomains
175 of the snapshot grid in the parameter space (see Fig.6).

176 For each of these evaluation points, an additional finite element calcu-
177 lation (snapshot) is performed on this point and the displacements of the

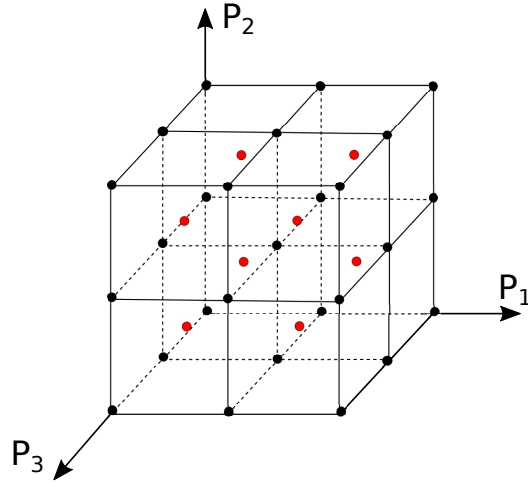


Figure 6: Example of a uniform grid with three values for each direction of the parameters P_1 to P_3 . The points in black are the finite element calculations and in red the evaluation points at the centers of the subdomains (cubes) formed by the discretization of the grid. The total represents $3^3 = 27$ snapshots and 8 evaluation points, in this example with three parameters. The method is generalizable to several parameters.

178 nodes of the distal part of the guidewire are stored in a reference U^{ref} ma-
 179 trix containing the so-called high fidelity results. The reduced model is used
 180 to interpolate the results on this point and the displacements obtained are in
 181 turn stored in a U matrix. For the considered point, an error δ is computed
 182 such that:

$$\delta = \frac{\|U - U^{ref}\|}{\|U^{ref}\|}$$

183 With $\|\bullet\|$ the L_2 norm.

184 2.2.4. Navigation assistance tools

185 2.2.4.1. Introduction.

186 The previous section deals with a specific tool dedicated to the designers of

187 the active guidewire and concerned exclusively the performance of the device.
188 In this part, more sophisticated numerical charts are proposed taking into
189 account both design and navigation parameters. These decision support tools
190 should allow to observe the navigation of the guide in a given anatomy for
191 various sets of parameters. Those developed in this section are proofs of
192 concept of decision support tools used in the preoperative phase. Their main
193 interest is the real time response. In the context of this work, the real time
194 is of the order of a second, comparable to the reaction time when using the
195 graphical interface. For integration of numerical chart in a medical robotics
196 environment, we will aim at a response time of the order of 0.1s maximum,
197 to be able to capture and control the fast movements of the tools.

198 *2.2.4.2. Endovascular navigation simulations in two typical anatomies.*

199 Two numerical charts are built taking into account endovascular navigation
200 in two typical aortas: the BH aorta, which is referred to as a standard aorta,
201 and the FM aorta, which is an aorta with a bovine arch (the left carotid
202 artery and the brachio-cephalic trunk share the same origin). The key steps
203 for the navigation into these aortas are illustrated Fig.7.

204 For navigation, the distal modulus is systematically activated at the be-
205 ginning of navigation to follow the shape of the arch and avoid the guidewire
206 to insert in the left subclavian artery. Therefore, the time of activation of
207 the distal modulus is not a parameter. The output data recorded are the dis-
208 placements of the distal part (73 mm blade) of the guidewire over time. The
209 data are saved every 0.01s of the simulation over a total simulation time of
210 10.6s and 11.5s for the BH and FM aorta, respectively. Using two 2.30 GHz
211 Xeon cores, the duration of a simulation is about 3h. A MatLab routine

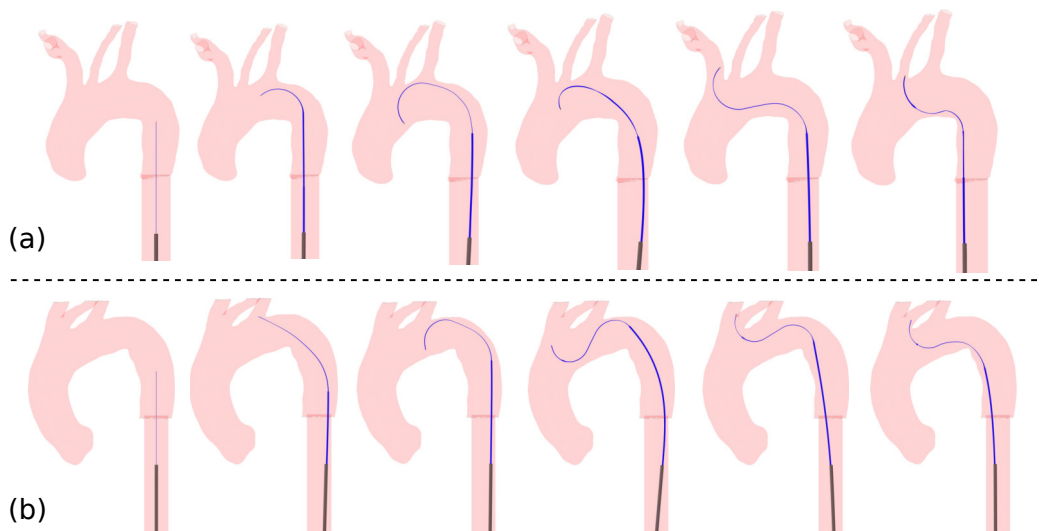


Figure 7: (a) Proposed navigation key steps for BH aorta hooking (standard aorta). The guidewire is pushed and the distal module is activated to prevent the device from inserting into the subclavian artery. After the guidewire is pushed, the proximal module is activated and snapping is initiated. The guidewire is then pulled. (b) The steps for navigation in the FM aorta (aorta with bovine arch) differ slightly: the guidewire navigates until it reaches the TSAs, the distal modulus is activated and snapping is triggered after the guidewire. The proximal modulus is then deactivated while pulling the guidewire to attempt to hook the carotid artery.

212 is also developed in this study to automatically generate the endovascular
 213 navigation model from selected parameters.

214 *2.2.4.3. Parameters.*

215 Among the design parameters, the focus is on that of the distal active modu-
 216 lus. Thus, the parameters L_d and ϵ_{L_d} which represent respectively the length
 217 of the distal module and the performance of the associated NiTi wire are
 218 included. Only the performance of the NiTi wire given by ϵ_{L_p} is selected to
 219 drive the design of the proximal modulus (L_p fixed at 27 mm and $e = 13$ mm).

220 The other four parameters concern navigation. The choice is made to
 221 focus on the guidewire pushing and pulling time (D_{push} and D_{pull}) and the
 222 time and duration of the activation of the proximal modulus (noted T_{actP}
 223 and D_{actP} respectively).

Table 2: Choice of the intervals for the seven parameters of the decision support charts. The intervals are given for the standard aorta case and with bovine arch.

<i>Parameters</i>	<i>Range of values for the standard aorta / with bovine arch</i>
L_d	[27 ; 32] / [27 ; 32]
ϵ_{L_p}	[0.026 ; 0.028] / [0.03 ; 0.033]
ϵ_{L_d}	[0.029 ; 0.033] / [0.033 ; 0.0347]
D_{push}	[2.0 ; 3.5] / [4.2 ; 5.2]
D_{pull}	[0.05 ; 1.5] / [1.7 ; 2.5]
T_{actP}	[3.5 ; 4.5] / [4.7 ; 5.3]
D_{actP}	[0.1 ; 0.6] / [1.8 ; 2.2]

224 *2.2.4.4. HOPGD enrichment and model accuracy.*

225 In the previous example, the error of the design aid abacus was used to
 226 get an idea of the accuracy of the response provided by the reduced model.
 227 For the decision support charts, the error of the reduced model will also be
 228 calculated and the chart will be dynamically improved by adding a control
 229 loop (refinement) during the learning phase. The general procedure is visible
 230 in Fig.8.

231 For the construction of these numerical abacuses, the generation of a
 232 uniform grid similar to the one used for the design aid abacus would have

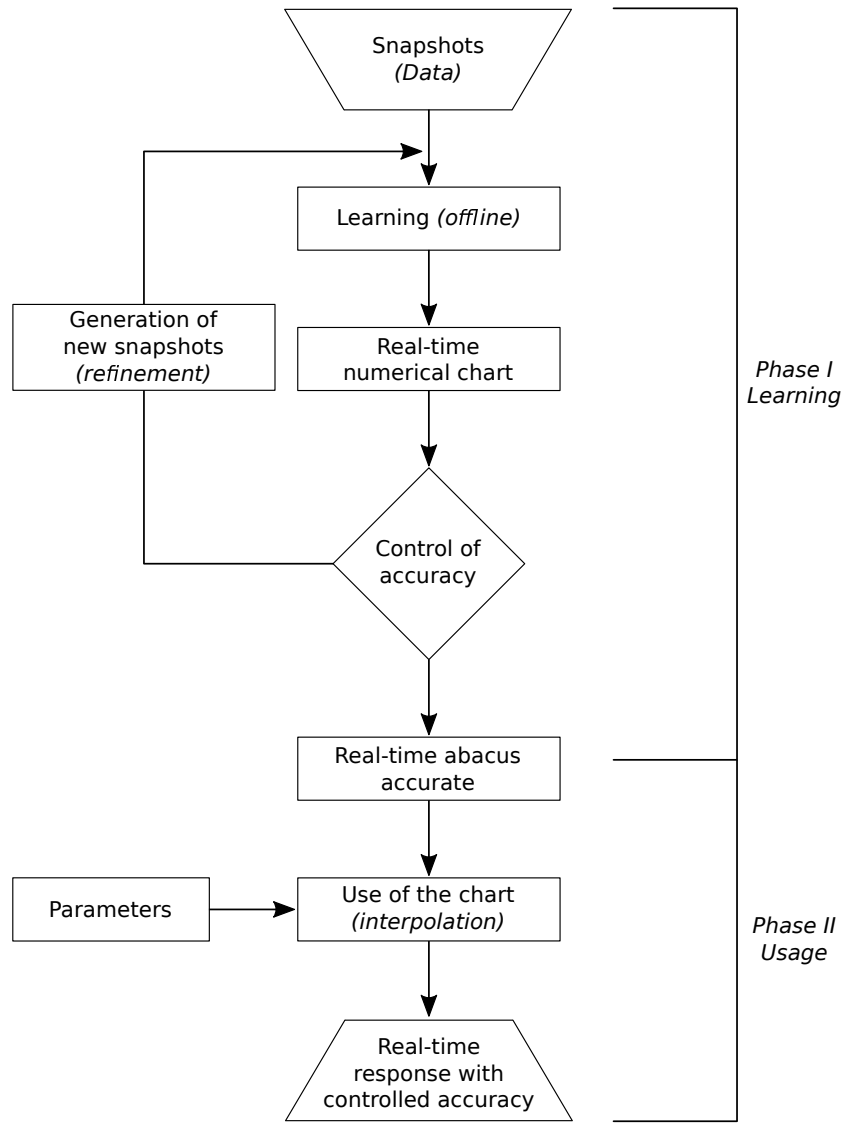


Figure 8: General procedure used for the development of decision support charts. From the snapshots computed in the parameter space in the learning phase, the reduced model is created and its accuracy is controlled. New snapshots are generated until the reduced model is considered as accurate enough. The real-time numerical chart is then used to give a real-time response given a set of parameters.

233 required $3^7 = 2187$ snapshots. A method is then proposed to limit the
 234 generation of too many snapshots while allowing the creation of charts with
 235 a satisfactory accuracy. The diagram Fig.9. shows an overview of the process.

236 As mentioned before, an additional procedure allows to determine the
 237 axes to be refined (addition of snapshots at the axis centers) when the
 238 error at the center of the hypercube is too important (greater than 5%).
 239 Let us note P^i the i -th parameter for $i = 1, \dots, 7$, P_{max}^i the maximum
 240 value that the parameter P^i takes (upper edge of the interval in Tab.2)
 241 and P_{middle}^i the middle of the interval of admissible values for the parame-
 242 ter P^i . Seven evaluation points are considered in order to determine which
 243 parameters most affect the error in the center of the hypercube. Each evalu-
 244 ation point evaluates the sensitivity of each parameter on the accuracy error
 245 of the chart. Thus, the first evaluation point has for set of parameters:
 246 $\{P_{middle}^1, P_{max}^2, P_{max}^3, P_{max}^4, P_{max}^5, P_{max}^6, P_{max}^7\}$, evaluating the contribution of
 247 the first parameter. In the same way the second evaluation point has the co-
 248 ordinates: $\{P_{max}^1, P_{middle}^2, P_{max}^3, P_{max}^4, P_{max}^5, P_{max}^6, P_{max}^7\}$ and so on. The error
 249 as a function of time is then calculated for each of these evaluation points.
 250 The parameter axes associated with evaluation points whose maximum er-
 251 ror exceeds 5% are refined by adding the midpoint on the parameter axis in
 252 question, for discretization of the snapshot grid.

253 In this part, we limit ourselves to a level 1 refinement (adding only one
 254 snapshot per direction) on three axes at most, which represents a final grid
 255 of $3^3 \times 2^3 = 432$ snapshots.

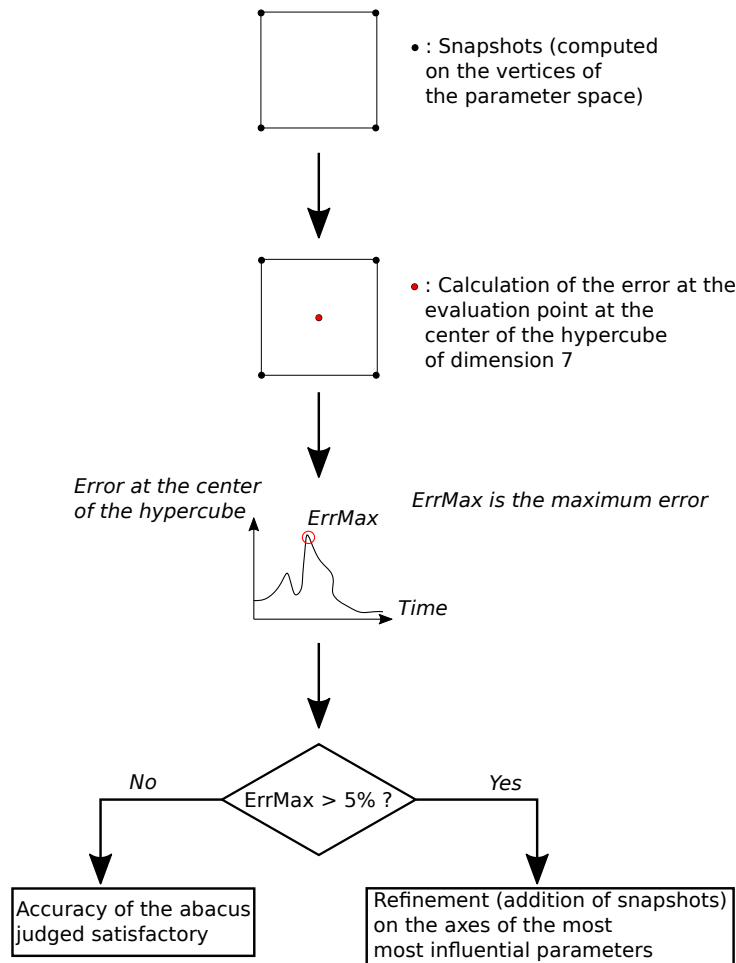


Figure 9: General procedure for the creation and enrichment of decision support charts on typical aortas (learning phase in Fig.8). The first step is to perform the simulations on the parameter sets at the vertices of the grid. The error during navigation is then evaluated at the center of the hypercube (dimension 7 here). When this error exceeds a threshold fixed at 5%, the discretization in the parameter space is densified on the axes of the influential parameters (addition of snapshots at the center of these axes). These parameters are chosen by a method evaluating their sensitivity on the error of the reduced model.

256 **3. Results**

257 *3.1. Active guidewire design tool*

258 From the 243 finite element calculations, the reduced model is created by
259 the HOPGD method in 17 seconds. The accuracy of the reduced model is
260 evaluated at the different centers of the subdomains of the parameter space,
261 i.e. on 32 evaluation points. The model is able to provide a solution in
262 10^{-5} s against 5 minutes by a finite element calculation on these points. The
263 percentage errors for the different centers are given Tab.3.

264 The reduced model allows to speed up considerably the computation time
265 and to create the numerical abacus visible on Fig.10. The graphical interface
266 is developed with Qt Creator (Qt Group, Finland). The set of parameters
267 chosen with the cursor interrogates the model and the interface displays the
268 corresponding guidewire displacements.

269 *3.2. Navigation assistance tools*

270 *3.2.1. Standard aorta*

271 From the snapshots at the grid vertices ($2^7 = 128$ snapshots), the reduced
272 model is created in 77 seconds. Using the method detailed in 2.2.4.4 to select
273 the axes to be refined, values at the centers of the axes of the parameters L_d ,
274 D_{pull} and T_{actP} are added, totaling a number of snapshots at $3^3 \times 2^4 = 432$.
275 With such a grid, the model is built in 263 seconds and the error at the
276 center of the hypercube is reduced (see Fig.11).

277 The performance, precision and parameters of the decision support tool
278 developed are summarized in Fig.12.

Table 3: Errors at the center of the subdomains of the 5 control parameters for the design aid chart.

<i>Subdomain number</i>	<i>Set of parameters</i>	<i>Error (in %)</i>
1	{15.5; 5.5; 20.5; 0.016175; 0.016175}	0.79
2	{18.5; 5.5; 20.5; 0.016175; 0.016175}	0.85
3	{15.5; 8.5; 20.5; 0.016175; 0.016175}	0.78
4	{18.5; 8.5; 20.5; 0.016175; 0.016175}	0.77
5	{15.5; 5.5; 33.5; 0.016175; 0.016175}	0.72
6	{18.5; 5.5; 33.5; 0.016175; 0.016175}	0.91
7	{15.5; 8.5; 33.5; 0.016175; 0.016175}	0.9
8	{18.5; 8.5; 33.5; 0.016175; 0.016175}	0.88
9	{15.5; 5.5; 20.5; 0.028525; 0.016175}	1.00
10	{18.5; 5.5; 20.5; 0.028525; 0.016175}	0.96
11	{15.5; 8.5; 20.5; 0.028525; 0.016175}	0.82
12	{18.5; 8.5; 20.5; 0.028525; 0.016175}	0.73
13	{15.5; 5.5; 33.5; 0.028525; 0.016175}	0.90
14	{18.5; 5.5; 20.5; 0.028525; 0.016175}	1.01
15	{15.5; 8.5; 33.5; 0.028525; 0.016175}	0.91
16	{18.5; 8.5; 33.5; 0.028525; 0.016175}	0.92
17	{15.5; 5.5; 20.5; 0.016175; 0.028525}	0.85
18	{18.5; 5.5; 20.5; 0.016175; 0.028525}	0.90
19	{15.5; 8.5; 20.5; 0.016175; 0.028525}	0.79
20	{18.5; 8.5; 20.5; 0.016175; 0.028525}	0.79
21	{15.5; 5.5; 33.5; 0.016175; 0.028525}	0.56
22	{18.5; 5.5; 33.5; 0.016175; 0.028525}	0.70
23	{15.5; 8.5; 33.5; 0.016175; 0.028525}	0.67
24	{18.5; 8.5; 33.5; 0.016175; 0.028525}	0.77
25	{15.5; 5.5; 20.5; 0.028525; 0.028525}	0.91
26	{18.5; 5.5; 20.5; 0.028525; 0.028525}	0.98
27	{15.5; 8.5; 20.5; 0.028525; 0.028525}	0.86
28	{18.5; 8.5; 20.5; 0.028525; 0.028525}	0.83
29	{15.5; 5.5; 33.5; 0.028525; 0.028525}	0.68
30	{18.5; 5.5; 33.5; 0.028525; 0.028525}	0.81
31	{15.5; 8.5; 33.5; 0.028525; 0.028525}	0.78
32	{18.5; 8.5; 33.5; 0.028525; 0.028525}	0.81

279 *3.2.2. Aorta with bovine arch*

280 The procedure is similar on this chart applied to a bovine arch anatomy.

281 The first model is built in 44 seconds but the error at the center of the

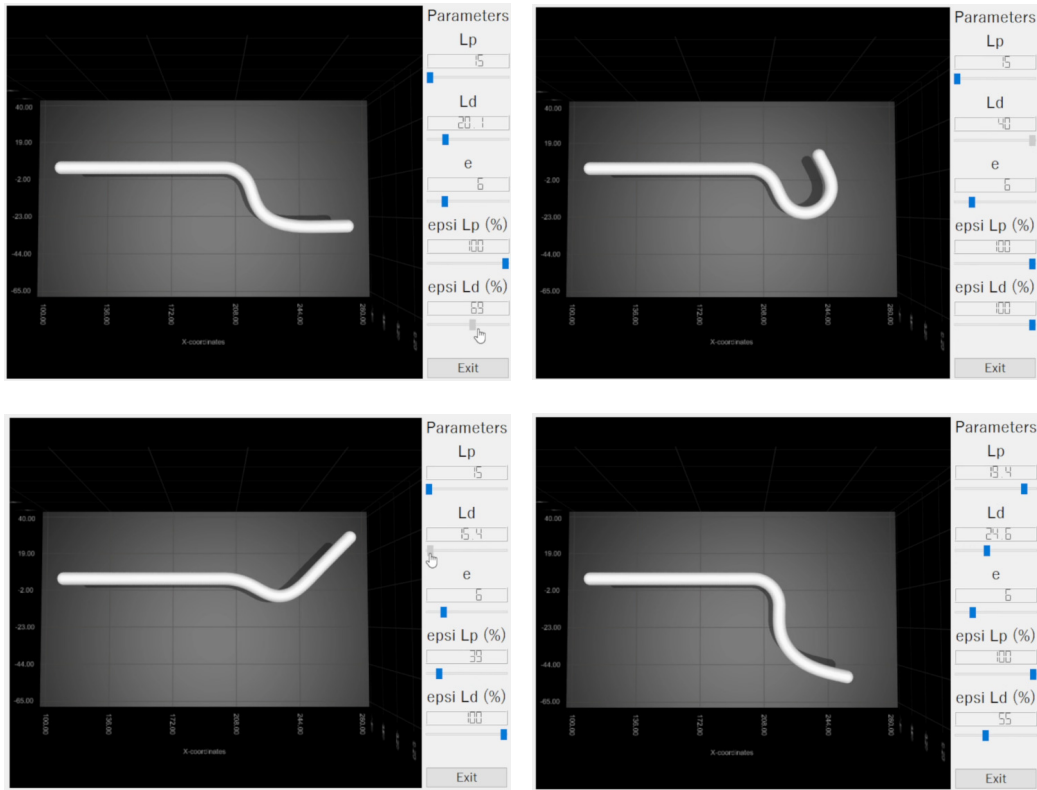


Figure 10: Numerical chart to help design the active guide. The five parameters can be modified and the tool allows to give a real time answer on the deformation of the guide with an accuracy of about 1%. A part of the rod is represented (left part of the rod) but has not been taken into account for the construction of the model. The figures represent different deformations of the guide according to the parameters chosen by the user on the right panel.

282 hypercube required a refinement on the axes of the parameters D_{pull} and
 283 T_{actP} leading to a model created in 164 seconds based on $3^2 \times 2^5 = 288$
 284 snapshots. The errors of the model before and after refinement are displayed
 285 Fig.13.

286 The main characteristics of the numerical chart with a fixed geometry of

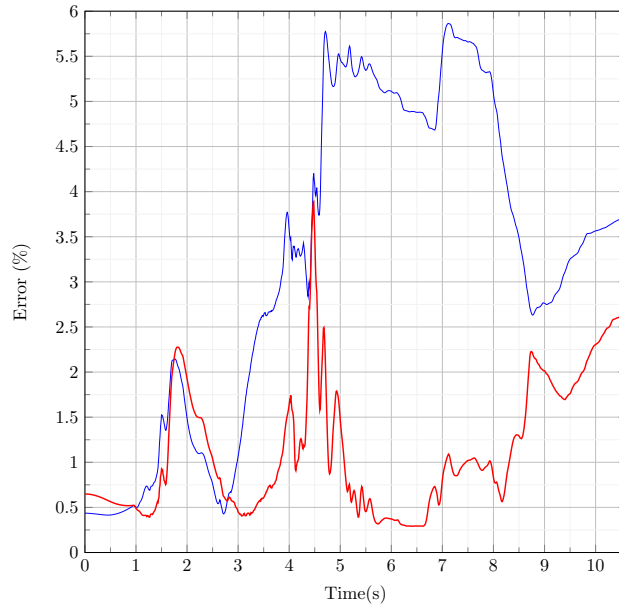


Figure 11: Error of the reduced model as a function of time, evaluated at the center of the hypercube in the parameter space. The blue curve refers to the reduced model computed on the basis of snapshots positioned at the vertices of the parameter space (128 snapshots). The red curve refers to the error of the reduced model for a grid with a denser discretization (432 snapshots). Case of the model used to create the standard aorta chart.

287 an aorta with bovine arch are summarized in Fig.14.

288 3.2.3. Conclusions on decision support charts

289 Overall, the charts show very satisfactory results. The snapping is cor-
 290 rectly replayed and the contact well represented. For each new set of parame-
 291 ters, the tools provide an instantaneous response (10^{-3} s) compared to nearly
 292 3 hours for a finite element calculation. The response time of the abacuses
 293 is well below the specifications.

294 Concerning the error curves in blue on the two charts (Fig.13 and 11), we
 295 observe peaks at key stages of the navigation. The first peak occurs when the

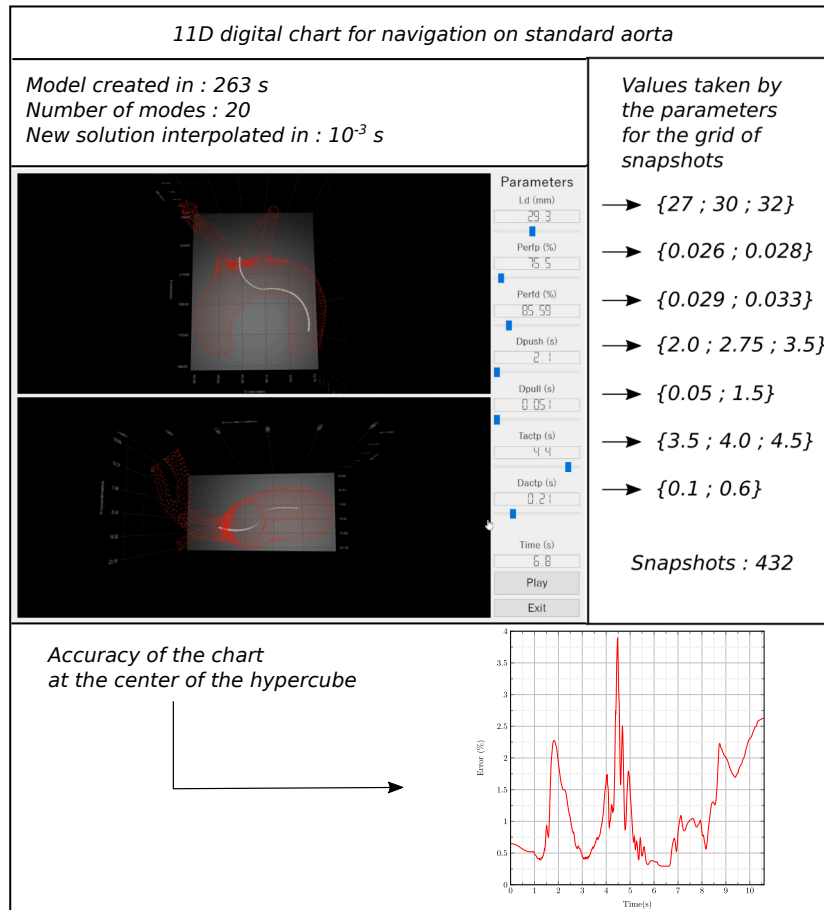


Figure 12: Assessment of the characteristics of the digital decision support chart on standard aorta.

296 distal module is activated. At the moment of snapping, the error increases
 297 sharply. For the first chart, this error gradually decreases and then increases
 298 again when the guide is pulled. The error curve of the second chart shows
 299 successive peaks during snapping, mainly due to high frequency vibrations
 300 of the guidewire. A second peak is visible when the proximal module is
 301 deactivated.

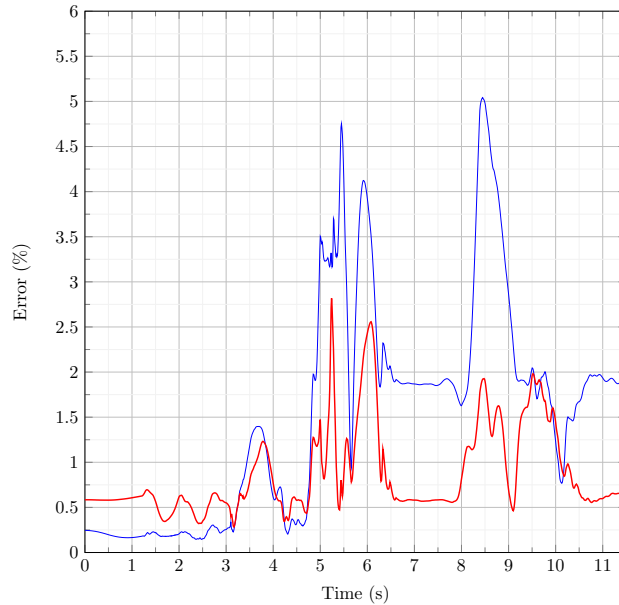


Figure 13: Error of the reduced model as a function of time evaluated at the center of the hypercube in the parameter space. The blue curve refers to the reduced model computed on the basis of snapshots positioned at the vertices of the parameter space (128 snapshots). The red curve refers to the error of the reduced model for a grid with a denser discretization (288 snapshots). Case of the model used to create the aorta with bovine arch chart.

302 4. Discussion

303 4.1. Main results

304 For the numerical charts, the choice was made for the HOPGD method.
 305 This method has proven to be efficient for problems with many parameters
 306 as it was the case in this study.

307 A first abacus to help the design has been developed. On this one, only
 308 guidewire design parameters were studied. Considering the simulation time
 309 of the snapshots used to create the reduced model and the preliminary tests,
 310 it was chosen to work on a uniform grid with three values per axis. Since the

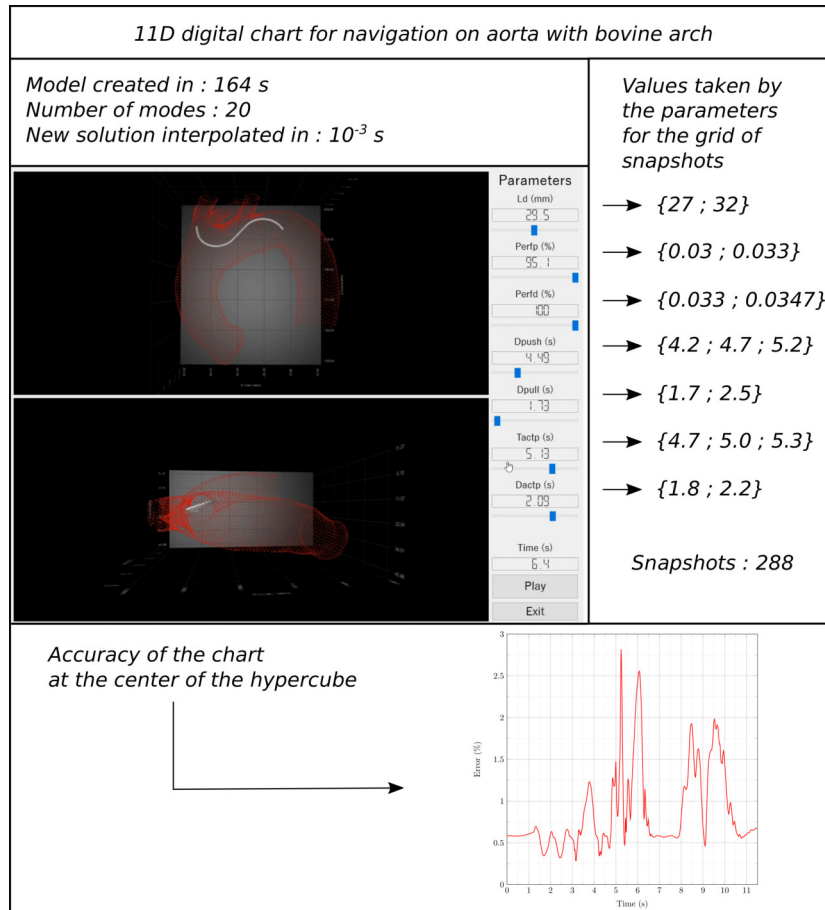


Figure 14: Assessment of the characteristics of the digital decision support chart on aorta with bovine arch.

311 intervals are relatively wide, the errors of the reduced model were evaluated
 312 at the centers of the subdomains formed by the grid.

313 In a second step, the objective was to work on more complex abacuses
 314 combining design and navigation parameters. These abacuses were intended
 315 to act as proofs of concept and to provide an insight into what could be
 316 achieved using model reduction methods in a biomechanical and in particular

317 cardiovascular framework.

318 Some remarks about the choice of the navigation parameters and the
319 values taken by each of them: these parameters are considered to be the most
320 influential for left carotid artery hooking. The extrema of these parameters
321 were determined by a preliminary analysis. With them, the guide navigates
322 between the origins of the left subclavian and the brachiocephalic trunk. The
323 extrema of these parameters are interdependent. Specifically, they follow the
324 navigation steps defined previously: for example, for navigation in the BH
325 aorta, the guidewire is first pushed, the proximal module is activated and
326 then the guidewire is pulled. The values do not overlap, and the abacus does
327 not allow in this study to explore other navigation steps.

328 In general, it was interesting to test the performance of the HOPGD
329 method in our problem associating nonlinearities, contact and fast phenom-
330 ena.

331 *4.2. Study limits*

332 Many tests (abacuses with less parameters, simulations to test the sen-
333 sitivity to some parameters) have been done beforehand and two main dif-
334 ficulties have been highlighted: the choice of parameters and their range of
335 values. The active guidewire was developed during this work. Consequently,
336 there was not the necessary hindsight to choose in an optimal way the pa-
337 rameters to be incorporated in the chart. We then relied on the experience
338 gained from the numerous simulations performed.

339 Concerning the values of the intervals, abacuses with two or three param-
340 eters allowed to show that too large intervals of values would require many
341 simulations. In order to develop proofs of concept and taking into account the

342 resources at our disposal, we set a maximum of 432 snapshots per abacus.
343 With seven control parameters, the selected value intervals were therefore
344 quite short and did not allow to explore large variations of the guidewire
345 navigation.

346 This main limitation came from the use of uniform grids. It would be
347 interesting to improve the generation of snapshots with a sparse grids method
348 to overcome this issue.

349 The errors for both decision support charts were evaluated at the cen-
350 ter of the hypercube. An error within 5% was considered satisfactory. This
351 criterion was determined by judging the displacements of the guidewire rel-
352 ative to the aorta: on the abacuses tested, a higher error corresponded to
353 poor management of the contact between the guidewire and the aorta, so the
354 guidewire tended to move away from the aorta. Moreover, the peaks occur
355 during the fast phenomena: activation and deactivation of the modules or
356 even snapping. A way to smooth the curves could be to record more data as
357 a function of time (reduction of the time step used to save the displacements
358 of the guidewire) in order to better capture these phenomena. However, it
359 would require a large amount of storage. It is observed after adding snapshots
360 (refinement) that the global error is clearly reduced with a better manage-
361 ment of the contact between the guide and the aorta, in particular when the
362 active device is pulled and the distal part hooks the aorta (end of the simula-
363 tion for both charts). The peaks persist for the red curves but with a clearly
364 attenuated amplitude. The accuracy is considered satisfactory considering
365 the relatively low number of snapshots for such a problem.

366 A method, adapted specifically for this study, allowed us to select the

367 axes to refine when this error exceeded 5%. For intervals with larger ex-
368 tremas, further analysis may be considered. For example, the errors could be
369 evaluated at the centers of the subdomains. From these results, the influ-
370 ential parameters could be identified and a refinement performed. The step
371 could be repeated for new subdomain centers and so on.

372 **5. Conclusion**

373 This study shows numerical charts for a design and decision support tools
374 dedicated to the use of the active guidewire. These solutions serve as a proof
375 of concept and show very promising results on the development of this type of
376 tool. Fixed anatomy abacuses were proposed in this study. A more powerful
377 tool could incorporate geometric parameters and allow, for a new patient, to
378 provide real-time decision support.

379 **6. Acknowledgements**

380 The French National Research Agency (ANR) partially supported this
381 work through the DEEP project: Devices for augmEnted Endovascular nav-
382 igation in complex Pathways (grant n°ANR-18-CE19-0027-01).

383 **7. Conflict of interest statement**

384 The authors declare that there are no conflicts of interest.

385 **References**

386 [1] R. Verhage, E. Hazebroek, J. Boone, R. van Hillegersberg, Minimally
387 invasive surgery compared to open procedures in esophagectomy for can-

- 388 cer: A systematic review of the literature, *Minerva chirurgica* 64 (2009)
389 135–46.
- 390 [2] S. Madhwal, V. Rajagopal, D. Bhatt, C. Bajzer, P. Whitlow, S. Kapadia,
391 Predictors of Difficult Carotid Stenting as Determined by Aortic Arch
392 Angiography, *J. Invasive. Cardiol.* 20 (2008) 200–4.
- 393 [3] A. Badrou, N. Tardif, P. Chaudet, N. Lescanne, J. Szewczyk, R. Blanc,
394 N. Hamila, A. Gravouil, A. Bel-Brunon, Simulation of multi-curve active
395 catheterization for endovascular navigation to complex targets, *Journal*
396 *of Biomechanics* 140 (2022) 111147.
- 397 [4] S. Kefayati, T. L. Poepping, Transitional flow analysis in the carotid
398 artery bifurcation by proper orthogonal decomposition and particle im-
399 age velocimetry, *Medical Engineering & Physics* 35 (7) (2013) 898–909.
- 400 [5] G. Janiga, Quantitative assessment of 4D hemodynamics in cerebral
401 aneurysms using proper orthogonal decomposition, *Journal of Biome-*
402 *chanics* 82 (2019) 80–86.
- 403 [6] A. Darwish, G. Di Labbio, W. Saleh, L. Kadem, Proper Orthogonal
404 Decomposition Analysis of the Flow Downstream of a Dysfunctional
405 Bileaflet Mechanical Aortic Valve, *Cardiovascular Engineering and Tech-*
406 *nology* 12 (3) (2021) 286–299.
- 407 [7] R. R. Rama, S. Skatulla, C. Sansour, Real-time modelling of diastolic
408 filling of the heart using the proper orthogonal decomposition with in-
409 terpolation, *International Journal of Solids and Structures* 96 (2016)
410 409–422.

- 411 [8] A. Barone, M. G. Carlino, A. Gizzi, S. Perotto, A. Veneziani, Efficient
412 estimation of cardiac conductivities: A proper generalized decomposi-
413 tion approach, *Journal of Computational Physics* 423 (2020) 109810.
- 414 [9] C. Quesada, D. González, I. Alfaro, E. Cueto, F. Chinesta, Computa-
415 tional vademecums for real-time simulation of surgical cutting in haptic
416 environments, *International Journal for Numerical Methods in Engi-
417 neering* 108 (10) (2016) 1230–1247.
- 418 [10] C. Quesada, I. Alfaro, D. González, F. Chinesta, E. Cueto, Haptic sim-
419 ulation of tissue tearing during surgery, *International Journal for Nu-
420 merical Methods in Biomedical Engineering* 34 (3) (2018) e2926.
- 421 [11] S. Niroomandi, D. González, I. Alfaro, F. Bordeu, A. Leygue, E. Cueto,
422 F. Chinesta, Real-time simulation of biological soft tissues: a PGD ap-
423 proach, *International Journal for Numerical Methods in Biomedical En-
424 gineering* 29 (5) (2013) 586–600.
- 425 [12] D. Modesto, S. Zlotnik, A. Huerta, Proper generalized decomposition
426 for parameterized Helmholtz problems in heterogeneous and unbounded
427 domains: Application to harbor agitation, *Computer Methods in Ap-
428 plied Mechanics and Engineering* 295 (2015) 127–149.
- 429 [13] Y. Lu, N. Blal, A. Gravouil, Multi-parametric space-time computational
430 vademecum for parametric studies: Application to real time welding
431 simulations, *Finite Elements in Analysis and Design* 139 (2018) 62–72.
- 432 [14] D. C. Lagoudas, *Shape Memory Alloys, Vol. 1*, Springer US, Boston,
433 MA, 2008.

- 434 [15] T. Couture, J. Szewczyk, Design and Experimental Validation of an Ac-
435 tive Catheter for Endovascular Navigation, *Journal of Medical Devices*
436 12 (Nov. 2017).
- 437 [16] L. R. Herrmann, F. E. Peterson, *A Numerical Procedure for Viscoelastic*
438 *Stress Analysis*, Orlando, Fl., 1968.
- 439 [17] Y. Lu, N. Blal, A. Gravouil, Adaptive sparse grid based HOPGD: To-
440 ward a nonintrusive strategy for constructing space-time welding com-
441 putational vademecum, *International Journal for Numerical Methods in*
442 *Engineering* 114 (13) (2018) 1438–1461.